

Atomic layer deposition of molybdenum oxide from (NtBu)₂(NMe₂)₂Mo and O₂ plasma

Citation for published version (APA):

Vos, M., Macco, B., Thissen, N. F. W., Bol, A. A., & Kessels, W. M. M. (2016). Atomic layer deposition of molybdenum oxide from (NtBu)₂(NMe₂)₂Mo and O₂ plasma. *Journal of Vacuum Science and Technology A*, 34(1), 01A103-1/8. Advance online publication. <https://doi.org/10.1116/1.4930161>

DOI:

[10.1116/1.4930161](https://doi.org/10.1116/1.4930161)

Document status and date:

Published: 01/01/2016

Document Version:

Publisher's PDF, also known as Version of Record (includes final page, issue and volume numbers)

Please check the document version of this publication:

- A submitted manuscript is the version of the article upon submission and before peer-review. There can be important differences between the submitted version and the official published version of record. People interested in the research are advised to contact the author for the final version of the publication, or visit the DOI to the publisher's website.
- The final author version and the galley proof are versions of the publication after peer review.
- The final published version features the final layout of the paper including the volume, issue and page numbers.

[Link to publication](#)

General rights

Copyright and moral rights for the publications made accessible in the public portal are retained by the authors and/or other copyright owners and it is a condition of accessing publications that users recognise and abide by the legal requirements associated with these rights.

- Users may download and print one copy of any publication from the public portal for the purpose of private study or research.
- You may not further distribute the material or use it for any profit-making activity or commercial gain
- You may freely distribute the URL identifying the publication in the public portal.

If the publication is distributed under the terms of Article 25fa of the Dutch Copyright Act, indicated by the "Taverne" license above, please follow below link for the End User Agreement:

www.tue.nl/taverne

Take down policy

If you believe that this document breaches copyright please contact us at:

openaccess@tue.nl

providing details and we will investigate your claim.

Atomic layer deposition of molybdenum oxide from (N t Bu)₂(NMe₂)₂Mo and O₂ plasma

Martijn F. J. Vos, Bart Macco, Nick F. W. Thissen, Ageeth A. Bol, and W. M. M. (Erwin) Kessels

Citation: *Journal of Vacuum Science & Technology A* **34**, 01A103 (2016); doi: 10.1116/1.4930161

View online: <http://dx.doi.org/10.1116/1.4930161>

View Table of Contents: <http://scitation.aip.org/content/avs/journal/jvsta/34/1?ver=pdfcov>

Published by the AVS: Science & Technology of Materials, Interfaces, and Processing

Articles you may be interested in

Atomic layer deposition of molybdenum oxide using bis(tert-butylimido)bis(dimethylamido) molybdenum

J. Vac. Sci. Technol. A **32**, 01A119 (2014); 10.1116/1.4843595

In situ reaction mechanism studies on the Ti(NMe₂)₂(OiPr)₂-D₂O and Ti(OiPr)₃[MeC(NiPr)₂]-D₂O atomic layer deposition processes

J. Vac. Sci. Technol. A **32**, 01A121 (2014); 10.1116/1.4843496

Combination of characterization techniques for atomic layer deposition MoO₃ coatings: From the amorphous to the orthorhombic α-MoO₃ crystalline phase


J. Vac. Sci. Technol. A **30**, 01A107 (2012); 10.1116/1.3643350

Reaction mechanisms during plasma-assisted atomic layer deposition of metal oxides: A case study for Al₂O₃



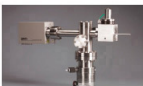
J. Appl. Phys. **103**, 103302 (2008); 10.1063/1.2924406

Impact of titanium addition on film characteristics of Hf O₂ gate dielectrics deposited by atomic layer deposition

J. Appl. Phys. **98**, 054104 (2005); 10.1063/1.2030407



Instruments for Advanced Science

| | | | | |
|---|--|--|--|--|
| <p>Contact Hiden Analytical for further details: W www.HidenAnalytical.com E info@hiden.co.uk</p> <p>CLICK TO VIEW our product catalogue</p> |  <p>Gas Analysis</p> <ul style="list-style-type: none"> › dynamic measurement of reaction gas streams › catalysis and thermal analysis › molecular beam studies › dissolved species probes › fermentation, environmental and ecological studies |  <p>Surface Science</p> <ul style="list-style-type: none"> › UHV TPD › SIMS › end point detection in ion beam etch › elemental imaging - surface mapping |  <p>Plasma Diagnostics</p> <ul style="list-style-type: none"> › plasma source characterization › etch and deposition process reaction › kinetic studies › analysis of neutral and radical species |  <p>Vacuum Analysis</p> <ul style="list-style-type: none"> › partial pressure measurement and control of process gases › reactive sputter process control › vacuum diagnostics › vacuum coating process monitoring |
|---|--|--|--|--|

Atomic layer deposition of molybdenum oxide from $(N^tBu)_2(NMe_2)_2Mo$ and O_2 plasma

Martijn F. J. Vos,^{a)} Bart Macco,^{a)} Nick F. W. Thissen, Ageeth A. Bol, and W. M. M. (Erwin) Kessels^{b)}

Department of Applied Physics, Eindhoven University of Technology, P.O. Box 513, 5600 MB Eindhoven, The Netherlands

(Received 24 July 2015; accepted 25 August 2015; published 9 September 2015)

Molybdenum oxide (MoO_x) films have been deposited by atomic layer deposition using bis(*tert*-butylimido)-bis(dimethylamido)molybdenum and oxygen plasma, within a temperature range of 50–350 °C. Amorphous film growth was observed between 50 and 200 °C at a growth per cycle (GPC) around 0.80 Å. For deposition temperatures of 250 °C and higher, a transition to polycrystalline growth was observed, accompanied by an increase in GPC up to 1.88 Å. For all deposition temperatures the O/Mo ratio was found to be just below three, indicating the films were slightly substoichiometric with respect to MoO_3 and contained oxygen vacancies. The high purity of the films was demonstrated in the absence of detectable C and N contamination in Rutherford backscattering measurements, and a H content varying between 3 and 11 at. % measured with elastic recoil detection. In addition to the chemical composition, the optical properties are reported as well. © 2015 American Vacuum Society. [<http://dx.doi.org/10.1116/1.4930161>]

I. INTRODUCTION

Molybdenum trioxide has received considerable interest due to its optical, electrical, and catalytic properties.^{1–4} Thin films of MoO_3 are being used in gas sensors,^{5,6} solid state lithium batteries,⁷ and in the synthesis of MoS_2 by sulfurization.⁸ Moreover, recently, MoO_3 has been used in organic photovoltaics,⁹ perovskite solar cells,¹⁰ and silicon solar cells as hole extraction layer.^{11–13}

A wide range of deposition techniques has been employed for the growth of MoO_3 films, such as thermal evaporation,¹⁴ electron beam evaporation,¹⁵ sputtering,^{16–18} chemical vapor deposition (CVD),¹⁹ and atomic layer deposition (ALD).^{9,20} Of these techniques, ALD offers the advantages of uniform and conformal growth, in conjunction with atomic level thickness control, merits which are highly desirable for some of the abovementioned applications. However, only few reports on ALD of MoO_3 can be found in literature. Diskus *et al.* deposited MoO_3 by ALD using molybdenum hexacarbonyl, $Mo(CO)_6$, as precursor and simultaneous doses of ozone and water as reactants.²⁰ However, the thermal stability of the $Mo(CO)_6$ precursor limited the ALD window to 152–172 °C. Another study used MoF_6 and Si_2H_6 for the ALD of molybdenum films, which were subsequently post-treated with UV/ozone to obtain fully oxidized MoO_3 .⁹ However, the fact that this is a two-step process that involves the use of a halide precursor makes this process less ideal. More recently, Bertuch *et al.* reported an ALD process to deposit MoO_x using bis(*tert*-butylimido)-bis(dimethylamido)-molybdenum, $(N^tBu)_2(NMe_2)_2Mo$, as the metal-organic precursor and ozone as reactant.²¹ This process promisingly shows a high growth per cycle (GPC) of ~ 1.3 Å at 300 °C, but suffers from a low GPC and from C and N contamination in the films at lower deposition temperatures of 150–200 °C.

Previously, the $(N^tBu)_2(NMe_2)_2Mo$ precursor has also been used by Miikkulainen *et al.* to grow films of molybdenum nitride using ammonia as reactant.²²

In this study, we report on an ALD process to deposit high-purity substoichiometric molybdenum trioxide (MoO_{3-x}) films using the $(N^tBu)_2(NMe_2)_2Mo$ precursor and O_2 plasma, for a wide temperature range of 50–350 °C. O_2 plasma can offer the advantage of reasonable growth rates at lower deposition temperatures. In recent work, we have already shown the potential of this process for the low-temperature deposition of selective hole contacts for silicon heterojunction solar cells.²³ Here, we extend the temperature range to 350 °C and provide a detailed study of the ALD process and material properties in general.

II. EXPERIMENT

A. Film deposition

MoO_x films were deposited in a home-built ALD reactor, consisting of a vacuum chamber connected to an inductively coupled plasma source and a pump unit. The pump unit consists of a rotary and turbomolecular pump reaching a base pressure of $\sim 10^{-6}$ Torr. An extensive description of the reactor can be found in earlier work from our group.²⁴ The typical processing conditions and experimental settings are summarized in Table I. The set temperature of the substrate table was varied between 50 and 350 °C. The temperature of the reactor wall was maintained at 100 °C, for all depositions, except for depositions at a table temperature of 50 °C, for which the wall temperature was set to 50 °C. The liquid $(N^tBu)_2(NMe_2)_2Mo$ precursor (98%, Strem Chemicals) was contained in a bubbler at 50 °C, at which it is reported to have a vapor pressure of 0.13 Torr.²¹ The chemical structure of the precursor can be seen in the inset of Fig. 1. The precursor supply line was heated to 80 °C to prevent condensation of the precursor and

^{a)}M. F. J. Vos and B. Macco contributed equally to this work.

^{b)}Electronic mail: w.m.m.kessels@tue.nl

TABLE I. Standard ALD recipe for the deposition of MoO_x. The Ar and O₂ pressure indicate the chamber pressure during Ar bubbling and plasma exposure, respectively. The reported deposition temperature is the set temperature of the substrate table.

| Parameter | Value |
|----------------------------|-----------------------|
| Deposition temperature | 50–350 °C |
| Wall temperature | 50–100 °C |
| Bubbler temperature | 50 °C |
| Precursor line temperature | 80 °C |
| Base pressure | 10 ⁻⁶ Torr |
| Ar pressure | 7.5 mTorr |
| O ₂ pressure | 5.1 mTorr |
| Precursor dosing time | 6.0 s |
| Precursor purge time | 3.0 s |
| Precursor pump time | 3.0 s |
| Plasma exposure time | 4.0 s |
| Reactant purge time | 3.0 s |

Ar was used as a carrier gas. All depositions were done on Si (100) wafers with native oxide.

The standard ALD recipe consists of precursor dosing for 6 s in the first half of the ALD cycle. Ar gas is used as a carrier gas during the precursor dose, resulting in a chamber pressure of 7.5 mTorr. Subsequently, the reactor is purged with Ar for 3 s and pumped down for 3 s. The second half-cycle consists of O₂ plasma exposure with a plasma power of 100 W at a chamber pressure 5.1 mTorr for 4 s.

B. Film analysis

The growth of the MoO_x films was monitored *in situ* by spectroscopic ellipsometry (SE) using a J.A. Woollam, Inc., M2000U ellipsometer. The dielectric function of the deposited films was parameterized using a combination of a Tauc-

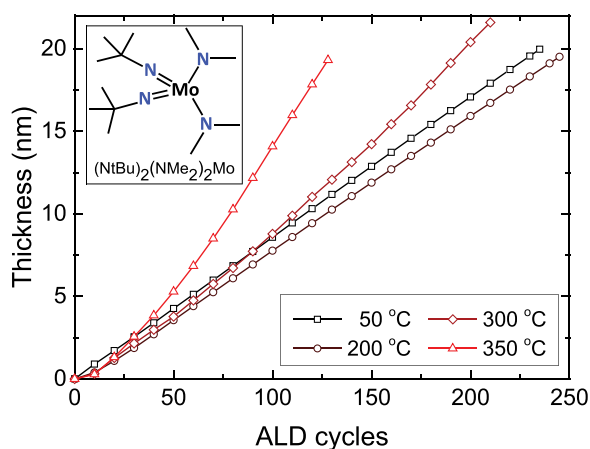


FIG. 1. (Color online) Thickness of the MoO_x films, measured with *in situ* SE, as a function of ALD cycles for deposition temperatures between 50 and 350 °C. A precursor dosing time of 6 s and plasma exposure time of 4 s were used. A transition from amorphous to polycrystalline growth can be observed for 300 and 350 °C by a gradual increase in GPC during film growth. The inset shows the chemical structure of the (NtBu)₂(NMe₂)₂Mo precursor used for the deposition. Some of the data in this figure has been replotted from previous work (Ref. 23).

Lorentz and a Gaussian oscillator, as will be addressed later in this paper.

X-ray photoelectron spectroscopy (XPS) was done with a Thermo Scientific KA1066 spectrometer, using monochromatic Al K α x-rays with an energy of 1486.6 eV. Rutherford backscattering spectroscopy (RBS) and elastic recoil detection (ERD) were performed by AccTec BV, Eindhoven, The Netherlands, using a Singletron with a 2 MeV He⁺ beam to determine the chemical composition of the films. The mass density was calculated using the areal mass density as obtained from RBS/ERD measurements and the film thickness as obtained from SE. Raman spectroscopy measurements were done using a Renishaw Invia Raman microscope, using a laser wavelength of 514 nm. Grazing incidence x-ray diffraction (XRD) measurements were done with a PANalytical X'Pert Pro MRD system, using Cu K α x-rays ($\lambda = 1.54 \text{ \AA}$). Scanning electron microscopy (SEM) images were obtained using a FEI Nova600i NanoLab.

III. RESULTS AND DISCUSSION

A. ALD growth

To study the ALD process as a function of the deposition temperature, a set of approximately 20 nm thick samples was deposited at temperatures between 50 and 350 °C, using a standard saturated precursor dosing time of 6 s and a plasma exposure time of 4 s. In Fig. 1, the film thickness is shown as a function of ALD cycles for temperatures between 50 and 350 °C. The thickness of the deposited films proceeds linearly with the number of ALD cycles for deposition temperatures of 50 and 200 °C, corresponding to a GPC of $\sim 0.8 \text{ \AA}$. For temperatures of 300 and 350 °C a gradual increase in GPC during film growth can be observed, which is attributed to a transition from amorphous to polycrystalline growth. Such a transition has been observed for other ALD processes before, for instance, for the deposition of TiO₂.^{25,26} A transition from amorphous to polycrystalline growth is accompanied by the appearance of grains, very likely leading to an increase in surface area and therefore to an increase in GPC. This will be further corroborated in Sec. III B 2, where the crystallinity and morphology of the films will be discussed.²⁷ Note that in addition to the increased roughness, an enhanced reactivity of the polycrystalline surface can also contribute to the increase in GPC. To exclude the presence of a thermal CVD component as a possible explanation for the enhanced growth rate at higher deposition temperatures, it was verified that no growth occurs when using O₂ gas instead of O₂ plasma as reactant.

In Fig. 2, the saturation curves for the precursor dose step [Fig. 2(a)] and plasma exposure time [Fig. 2(b)] are shown for various temperatures. The GPC as a function of precursor dosing time [Fig. 2(a)] shows a relatively soft saturation and a precursor dosing time of 6 s was chosen as standard for all deposition temperatures. The plasma saturation curve [Fig. 2(b)] shows a slightly higher GPC for low plasma exposure times, likely corresponding to incomplete combustion of precursor ligands or redeposition.²⁸ To assure complete combustion of ligands and to prevent impurity incorporation in

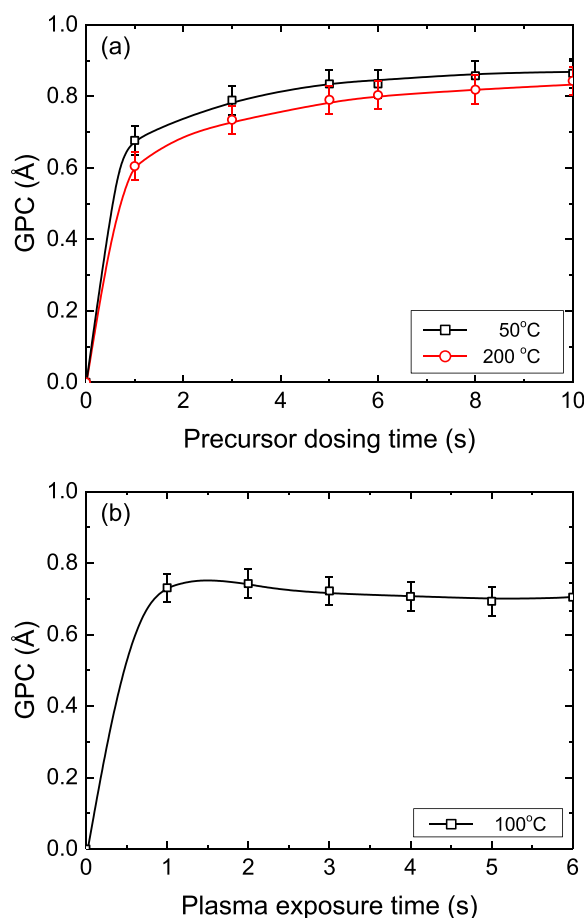


Fig. 2. (Color online) (a) Precursor saturation curve showing the GPC as a function of precursor dosing time for a constant plasma exposure time of 4s. (b) Plasma exposure saturation curve for a deposition temperature of 100 °C depicting the GPC as a function of plasma exposure time. The precursor dosing time was kept constant at 6 s. The lines serve as guides to the eye. Some of the data in this figure has been replotted from previous work (Ref. 23).

the films a plasma exposure time of 4 s was chosen as standard.

In Fig. 3, the GPC as a function of deposition temperature is shown, both in terms of thickness, determined from SE, and in terms of deposited Mo atoms/nm², determined from RBS. Note that the samples used for determination of the GPC data in Fig. 3 correspond to the samples used in Fig. 1 and had a thickness of ~20 nm. As can be seen in Fig. 3, the GPC determined by SE (closed squares) varies only slightly for temperatures between 50 and 200 °C. At these deposition temperatures, the films are completely amorphous (see Sec. III B 2). For higher temperatures, the GPC increases, which is due to a transition to polycrystalline growth. For a deposition temperature of 300 °C, a distinction can be made between amorphous growth at the start of the deposition, and polycrystalline growth at a larger film thickness, as is also shown in Fig. 3. The GPC determined from the first 20–100 cycles was found to be 0.93 Å, while calculating the GPC from the last 50 cycles of the deposition at 300 °C yields a GPC of 1.25 Å. Note that these values for the GPC were calculated by determining the slope at different positions on the curves in Fig. 1. Since at 350 °C the amorphous-polycrystalline transition occurs already at a very early stage,

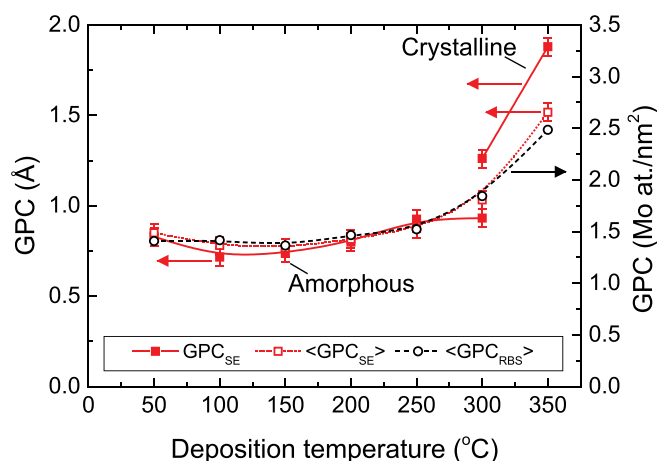


Fig. 3. (Color online) GPC in terms of thickness from *in situ* SE (left axis) and GPC in terms of deposited Mo atoms/nm² (right axis) from *ex situ* RBS, as a function of deposition temperature. The open circles show the average GPC in terms of deposited Mo atoms/nm², determined by division of the total Mo atoms/nm² by the number of ALD cycles. The open squares depict the average GPC ($\langle\text{GPC}_{\text{SE}}\rangle$), determined from the final thickness and the number of cycles, while the solid squares show the final GPC (GPC_{SE}), determined using the *in situ* data of the last 50 cycles of the deposition. In addition, a GPC determined before the onset of polycrystalline growth (<100 cycles) is displayed for a deposition temperature of 300 °C. The lines are a guide to the eye. The relative error in the measured number of Mo atoms is 2%.

only the GPC for polycrystalline growth is reported for this temperature.

Figure 3 also shows the GPC in terms of the number of deposited Mo atoms/nm² (open circles), as determined from RBS, which shows an increase with temperature. Note that this value was determined *ex situ* by dividing the total number of Mo atoms/nm² by the number of ALD cycles. The value is therefore an average over all the ALD cycles used to deposit the film. For this reason this quantity is denoted as $\langle\text{GPC}_{\text{RBS}}\rangle$. For a direct comparison of the RBS and SE data, also the average GPC as determined from SE ($\langle\text{GPC}_{\text{SE}}\rangle$), which is the final film thickness divided by the total number of cycles, is shown in Fig. 3 (open squares). As can be seen, there is a very strong correlation between $\langle\text{GPC}_{\text{RBS}}\rangle$ and $\langle\text{GPC}_{\text{SE}}\rangle$, which demonstrates that the increased GPC at high temperatures is mainly caused by an actual increase in the number of deposited Mo atoms per cycle and not by a decrease in film density. This increase in GPC at high temperatures is thought to be caused by an increase in surface area due to increased roughness, an increased reactivity of the surface, or a combination of both.²⁷

B. Film characterization

In this section, the chemical composition, morphology, and optical properties of the ~20 nm films deposited at temperatures between 50 and 350 °C will be discussed. The most important film properties have been summarized in Table II.

1. Chemical composition

From RBS/ERD measurements, both the stoichiometry and the elemental composition were determined. The O/Mo ratio and the atomic percentage of H as a function of

TABLE II. Properties of MoO_x films for deposition temperatures 50–350 °C, as determined from RBS, SE, and XPS. The thickness of the films was approximately 20 nm and the GPC was determined from the last 50 cycles of the deposition. The number of deposited Mo at. nm⁻² cycle⁻¹ and the chemical composition were determined from RBS, the refractive index and the Tauc band gap (E_g) from SE and the density from combining the RBS and SE results. C and N contamination in the bulk were below the RBS detection limit of 3 and 2 at. %, respectively. Typical errors are indicated in the top row and in the third row for the H content.

| Deposition temperature (°C) | GPC (Å) | Mo (at. nm ⁻² cycle ⁻¹) | O/Mo | [H] (at. %) | Mass density (g cm ⁻³) | Refractive index (at 1.96 eV) | E _g (eV) |
|-----------------------------|-------------|--|-----------|-------------|------------------------------------|-------------------------------|---------------------|
| 50 | 0.83 ± 0.03 | 1.41 ± 0.05 | 2.9 ± 0.1 | 11 ± 1 | 3.9 ± 0.2 | 2.11 ± 0.03 | 2.87 ± 0.03 |
| 100 | 0.72 | 1.42 | 2.8 | 10 | 4.3 | 2.20 | 2.80 |
| 150 | 0.74 | 1.37 | 2.9 | 3.3 ± 0.4 | 4.2 | 2.19 | 2.81 |
| 200 | 0.80 | 1.47 | 2.9 | 3.3 | 4.2 | 2.18 | 2.80 |
| 250 | 0.93 | 1.52 | 3.0 | 3.6 | 4.2 | 2.13 | 2.77 |
| 300 | 1.25 | 1.84 | 2.9 | 4.3 | 4.2 | 2.12 | 2.92 |
| 350 | 1.88 | 2.48 | 2.9 | 4.1 | 3.9 | 1.98 | 2.92 |

deposition temperature can be found in Table II. The O/Mo ratio was found to be below 3 for all investigated deposition temperatures (2.9 on average), indicating the films were slightly substoichiometric with respect to molybdenum trioxide (O/Mo ratio = 3). Note that the samples were transferred in ambient and therefore an effect of ambient on the film stoichiometry cannot be excluded. For all deposition temperatures the contents of C and N impurities were below the detection limit of 3 and 2 at. %, respectively, showing the high quality of the films. No substantial C or N contamination is present in the bulk of the films, which is in line with the fact that there is no indication of thermal decomposition of the precursor molecule for high decomposition temperatures. The H content of the films deposited at 50 and 100 °C was found to be around 10 at. %, which decreased to ~5 at. % for higher temperatures. This H can originate from the ligands of the precursor molecule, which contains 30 H atoms, as well as from residual water in the reactor.

The mass density of the films was calculated using the RBS/ERD measurements and the layer thicknesses from SE. For deposition temperatures from 100 to 300 °C the density was found to be around 4.2 g cm⁻³, which is slightly lower than the bulk density of crystalline MoO₃ of 4.69 g cm⁻³. The density is somewhat lower (3.9 g cm⁻³) for 50 and 350 °C.

XPS was used to further study the chemical composition of the deposited films. In Fig. 4(a), the Mo3d peak is depicted for a deposition temperature of 50 and 350 °C. It was found that sputtering of MoO_x with Ar ions causes a change in stoichiometry of the material due to preferential O sputtering, which is known from literature.²⁹ For this reason, the XPS data in Fig. 4 were collected prior to any sputtering, and thus, the presence of surface contamination cannot be excluded.

The Mo3d XPS spectrum in Fig. 4(a) shows a dominant doublet with the Mo3d_{5/2} peak at ~233.0 eV and the Mo3d_{3/2} peak at 236.2 eV, corresponding to the fully oxidized Mo⁶⁺ state, i.e., MoO₃.^{29,30} The binding energy of the Mo3d_{5/2} peak is slightly higher than other literature reports, which is likely an effect of surface charging.¹⁷ A second doublet at 231.7 and 235.0 eV is required to obtain a good fit to the experimental data. This doublet has previously been attributed

to the Mo⁵⁺ state, corresponding to oxygen vacancies.^{11,31} For instance, Battaglia *et al.* demonstrated an increase in the Mo⁵⁺ peak upon annealing the samples in N₂ environment, whereas no change was observed when annealing in O₂ environment.¹¹ Similar experiments were carried out in this study and yielded similar results, showing an increase in the Mo⁵⁺ state and even the appearance of the Mo⁴⁺ state upon annealing at 500 °C in N₂ environment (not shown here). The presence of oxygen vacancies is also consistent with the

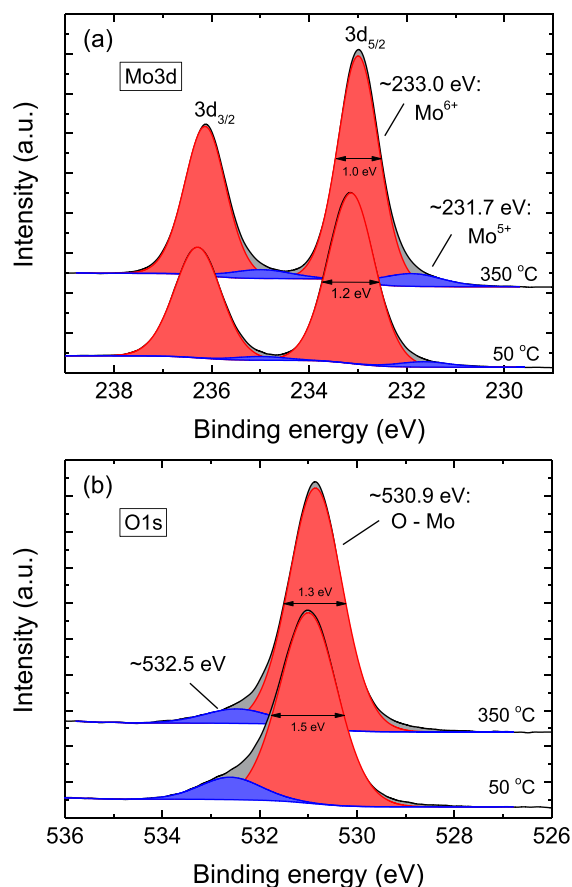


Fig. 4. (Color online) XPS core level spectra for Mo3d (a) and O1s (b) for MoO_x deposited at 50 and 350 °C. The data was obtained prior to Ar sputtering to avoid reduction of Mo to lower oxidation states.

substoichiometric O/Mo ratio as was found with RBS. The O1s peak in Fig. 4(b) consists of a dominant peak at approximately 530.9 eV, corresponding to O bound to Mo atoms²⁹ and a small shoulder around 532.5 eV, which could possibly be explained by O–H bonds³¹ or by absorbed surface species.¹⁷ Although the presence of C and N was observed in the XPS spectrum, their signals were almost completely absent after shortly sputtering with Ar⁺ ions. This indicates that C and N were mainly present on the surface, which is consistent with the RBS results.

2. Crystallinity and surface morphology

Raman spectroscopy and XRD were used to assess the crystallinity of the films as a function of the deposition temperature. From Fig. 5(a) it can be seen that the film deposited at 250 °C shows two peaks, at 777 and 849 cm⁻¹, corresponding to the metastable monoclinic β -crystal phase.^{32,33} For 300 and 350 °C a clear peak is visible at 818 cm⁻¹, indicating the films are in the stable orthorhombic α -phase. The absence of these peaks for temperatures of 200 °C and lower confirms their amorphous nature. The x-ray diffractograms

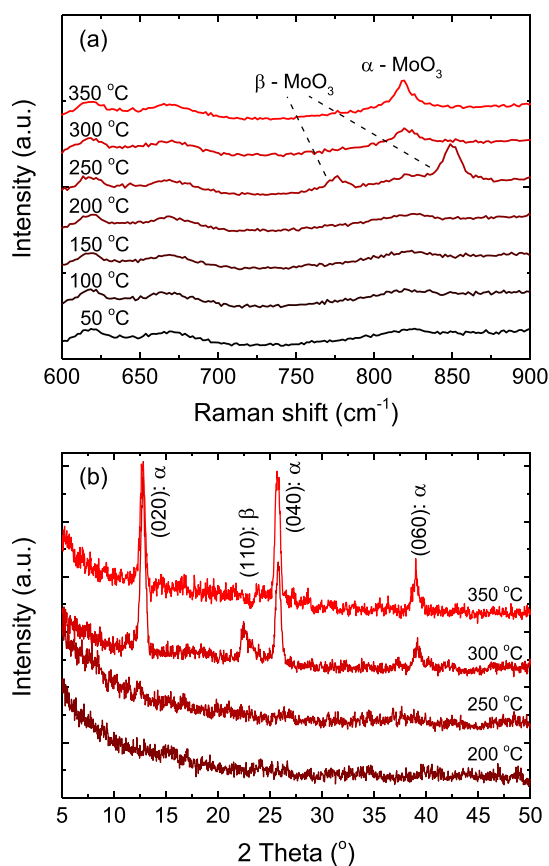


Fig. 5. (Color online) Raman spectra of the MoO_x films deposited at temperatures between 50 and 350 °C, for films of approximately 20 nm thick. At 250 °C the monoclinic β -phase of MoO₃ is visible, while films deposited at 300 and 350 °C show features of the orthorhombic α -phase. (b) X-ray diffractograms of the \sim 20 nm thick MoO_x films deposited at temperatures between 200 and 350 °C. For 300 and 350 °C distinct peaks are visible, corresponding to crystalline material, while the spectra for lower temperatures indicate the films are amorphous. The spectra are offset vertically for clarity.

in Fig. 5(b) show similar results of crystalline films at higher deposition temperatures. The (110) peak in Fig. 5(b) corresponds to the β -phase, while the (020), (040), and (060) peaks originate from the α -phase.³⁴ For 300 °C the Raman spectrum in Fig. 5(a) only shows the presence of the α -phase, while the x-ray diffractogram in Fig. 5(b) shows mainly the α -phase, with a small additional contribution originating from the β crystal-phase. For 200 and 250 °C no peaks are visible, corresponding to amorphous material.

Although Raman spectroscopy shows crystallinity for a deposition temperature of 250 °C it is thought that the bulk material is amorphous and some small crystallites are present at the surface of the film. This can also be seen in the SEM images in Fig. 6.

The film morphology as a function of deposition temperature was studied by top-view SEM (Fig. 6). For a deposition temperature of 50 °C, a relatively smooth surface is observed, corresponding to amorphous film growth. At 250 °C, some small nuclei are visible, surrounded by amorphous material. The film deposited at 300 °C contains many, larger crystallites, but amorphous material is still visible in the background. For 350 °C, the surface of the film appears fully crystalline. The appearance of crystallites and increasing crystallinity at higher temperatures is in agreement with the Raman data as presented in Fig. 5, as well as the observations made based on Fig. 1. Moreover, the increased roughness at higher deposition temperatures was also confirmed with atomic force microscopy (not shown), which showed a RMS roughness of 0.2 nm for 50 °C vs 1.9 nm for 350 °C.

3. Optical properties

The optical properties of the MoO_x films have been analyzed using SE. A Tauc-Lorentz oscillator was used to account for interband absorption. Additionally, a Gaussian oscillator at low photon energy (\sim 1 eV) was used for absorption inside the band gap, likely caused by defects. This absorption at low photon energy has been reported earlier for MoO_x and has been attributed to oxygen defects.^{4,11,16,35}

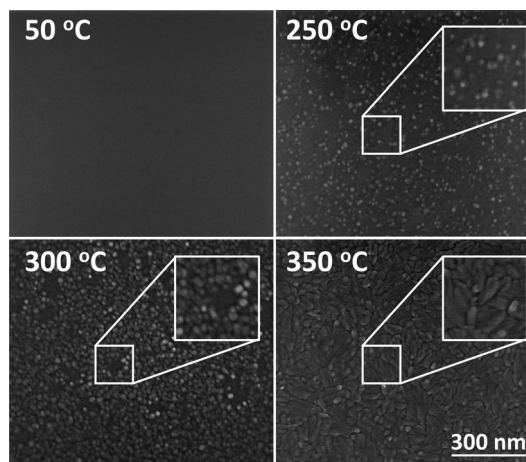


Fig. 6. Top-view SEM images of samples deposited at 50, 200, 300, and 350 °C. The thickness of the films was approximately 20 nm. For the three higher temperatures an area is shown at higher magnification for clarity.

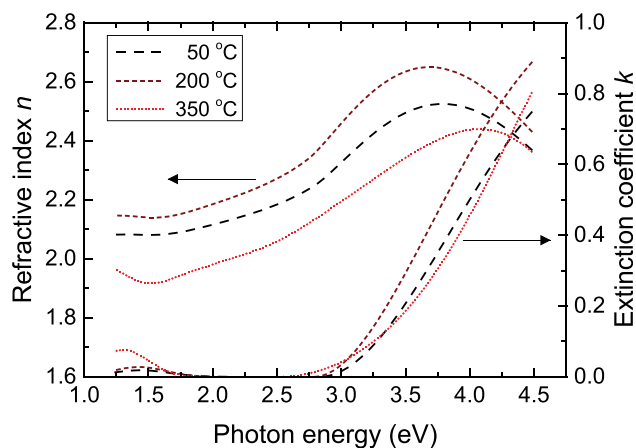


FIG. 7. (Color online) Refractive index (n) and extinction coefficient (k) for samples deposited at temperatures of 50, 200, and 350 °C. The data was obtained from *in situ* SE measurements. A Tauc-Lorentz oscillator was used to account for interband absorption, while an additional Gaussian oscillator at ~ 1.3 eV was used for subgap absorption. The Gaussian oscillator has been attributed to oxygen-vacancy-derived defects (Refs. 4, 11, 16, and 35).

The refractive index (n) and the extinction coefficient (k) obtained from the modeling are shown in Fig. 7.

The refractive index in Fig. 7 lies in the 1.8–2.2 range, which is consistent with other literature on MoO_x .^{16,36} Although the extinction coefficient k varies only slightly with deposition temperature, the refractive index n is strongly dependent on the deposition temperature, likely caused by differences in film density. From the absorption coefficient α obtained from the SE measurements the Tauc band gap was determined by plotting $(\alpha h\nu)^{1/2}$ as a function of photon energy (considering MoO_x is an indirect band gap material) and extrapolating the linear part to zero absorption.³⁷ The results of this procedure are listed in Table II. The obtained band gap values of 2.7–2.9 eV are in the range of the values of 2.5–3.0 eV previously reported in the literature.^{1,2,36,38} For deposition temperatures of 300 and 350 °C, a slightly higher band gap of 2.9 eV than for lower deposition temperatures was found, which is in line with the polycrystalline nature of the material.

IV. SUMMARY AND CONCLUSIONS

An ALD process to deposit high-purity MoO_x films has been presented, which is based on $(\text{N}^t\text{Bu})_2(\text{NMe}_2)_2\text{Mo}$ dosing and O_2 plasma exposure and which yields a high GPC over a temperature range of 50–350 °C. For amorphous growth at low temperature (<250 °C), GPC values of 0.72–0.93 Å were obtained. For higher deposition temperatures, a transition to polycrystalline growth occurs, which is accompanied by an increase in GPC up to 1.88 Å for 350 °C. It was shown that this increase in GPC is consistent with an increase in the amount of deposited Mo at nm^{-2} cycle⁻¹. For all deposition temperatures the MoO_x films were found to be slightly substoichiometric with respect to MoO_3 . Contamination by C and N was determined to be below the RBS detection limit of 3 and 2 at. %, respectively, which

shows the high quality of the material. In addition, the MoO_x films contain 3–11 at. % hydrogen. The Tauc band gap was found to vary between 2.77 and 2.87 eV for amorphous films and was 2.92 eV for polycrystalline films deposited at 300 and 350 °C.

Due to the high purity of the films and the relatively high GPC, the presented process is likely suitable for many applications, such as photovoltaics and other optoelectronic devices.

ACKNOWLEDGMENTS

The authors gratefully acknowledge Cristian van Helvoirt and Caspar van Bommel for technical assistance, Harm Knoop for fruitful discussion and Akhil Sharma for his assistance with the SEM analysis. This work was financially supported by the Dutch Technology Foundation STW through the Flash Perspectief Programma. The research of one of the authors (W.M.M.K.) has been made possible by the Dutch Technology Foundation STW and the Netherlands Organization for scientific Research (NWO, VICI Programme).

- ¹T. He and J. Yao, *J. Photochem. Photobiol. C* **4**, 125 (2003).
- ²T. Ivanova, K. A. Gesheva, G. Popkirov, M. Ganchev, and E. Tzvetkova, *Mater. Sci. Eng. B* **119**, 232 (2005).
- ³J. Scarminio, A. Lourenço, and A. Gorenstein, *Thin Solid Films* **302**, 66 (1997).
- ⁴T. S. Sian and G. B. Reddy, *Sol. Energy Mater. Sol. Cells* **82**, 375 (2004).
- ⁵M. Ferroni, V. Guidi, G. Martinelli, P. Nelli, M. Sacerdoti, and G. Sberveglieri, *Thin Solid Films* **307**, 148 (1997).
- ⁶O. M. Hussain and K. S. Rao, *Mater. Chem. Phys.* **80**, 638 (2003).
- ⁷H. Ohtsuka and Y. Sakurai, *Solid State Ionics* **144**, 59 (2001).
- ⁸Y. C. Lin, W. Zhang, J. K. Huang, K. K. Liu, Y. H. Lee, C. Te Liang, C. W. Chu, and L. J. Li, *Nanoscale* **4**, 6637 (2012).
- ⁹Y. C. Tseng, A. U. Mane, J. W. Elam, and S. B. Darling, *Sol. Energy Mater. Sol. Cells* **99**, 235 (2012).
- ¹⁰Y. Zhao, A. M. Nardes, and K. Zhu, *Appl. Phys. Lett.* **104**, 213906 (2014).
- ¹¹C. Battaglia *et al.*, *Nano Lett.* **14**, 967 (2014).
- ¹²C. Battaglia, S. M. de Nicolás, S. De Wolf, X. Yin, M. Zheng, C. Ballif, and A. Javey, *Appl. Phys. Lett.* **104**, 113902 (2014).
- ¹³J. Bullock, A. Cuevas, T. Allen, and C. Battaglia, *Appl. Phys. Lett.* **105**, 232109 (2014).
- ¹⁴T. Siciliano, A. Tepore, E. Filippo, G. Micocci, and M. Tepore, *Mater. Chem. Phys.* **114**, 687 (2009).
- ¹⁵R. Sivakumar, R. Gopalakrishnan, M. Jayachandran, and C. Sanjeeviraja, *Curr. Appl. Phys.* **7**, 51 (2007).
- ¹⁶S. H. Mohamed and S. Venkataraj, *Vacuum* **81**, 636 (2007).
- ¹⁷C. V. Ramana, V. V. Atuchin, V. G. Kesler, V. A. Kochubey, L. D. Pokrovsky, V. Shutthanandan, U. Becker, and R. C. Ewing, *Appl. Surf. Sci.* **253**, 5368 (2007).
- ¹⁸S. Uthanna, V. Nirupama, and J. F. Pierson, *Appl. Surf. Sci.* **256**, 3133 (2010).
- ¹⁹K. A. Gesheva, A. Cziraki, T. Ivanova, and A. Szekeres, *Thin Solid Films* **515**, 4609 (2007).
- ²⁰M. Diskus, O. Nilsen, and H. Fjellvåg, *J. Mater. Chem.* **21**, 705 (2011).
- ²¹A. Bertuch, G. Sundaram, M. Saly, D. Moser, and R. Kanjolia, *J. Vac. Sci. Technol. A* **32**, 01A119 (2014).
- ²²V. Miikkulainen, M. Suvanto, and T. A. Pakkanen, *Chem. Mater.* **19**, 263 (2006).
- ²³B. Macco, M. F. J. Vos, N. F. W. Thissen, A. A. Bol, and W. M. M. Kessels, *Phys. Status Solidi RRL* **9**, 393 (2015).
- ²⁴S. B. S. Heil, E. Langereis, F. Roozeboom, M. C. M. van de Sanden, and W. M. M. Kessels, *J. Electrochem. Soc.* **153**, G956 (2006).
- ²⁵A. Aarik, J. Karlis, H. Mändar, T. Uustare, and V. Sammelselg, *Appl. Surf. Sci.* **181**, 339 (2001).
- ²⁶J. Aarik, A. Aidla, H. Mändar, and V. Sammelselg, *J. Cryst. Growth* **220**, 531 (2000).

- ²⁷O. Nilsen, O. B. Karlsen, A. Kjekshus, and H. Fjellvåg, *Thin Solid Films* **515**, 4538 (2007).
- ²⁸H. C. M. Knoops, K. de Peuter, and W. M. M. Kessels, *Appl. Phys. Lett.* **107**, 014102 (2015).
- ²⁹F. Werfel and E. Minni, *J. Phys. D Solid State Phys.* **16**, 6091 (1983).
- ³⁰J. G. Choi and L. T. Thompson, *Appl. Surf. Sci.* **93**, 143 (1996).
- ³¹M. Vasilopoulou *et al.*, *J. Am. Chem. Soc.* **134**, 16178 (2012).
- ³²E. Haro-Poniatowski, M. Jouanne, J. F. Morhange, C. Julien, R. Diamant, M. Fernández-Guasti, G. A. Fuentes, and J. C. Alonso, *Appl. Surf. Sci.* **127–129**, 674 (1998).
- ³³L. Seguin, M. Figlarz, R. Cavagnat, and J. C. Lassègues, *Spectrochim. Acta Part A* **51**, 1323 (1995).
- ³⁴S.-Y. Lin, Y.-C. Chen, C.-M. Wang, P.-T. Hsieh, and S.-C. Shih, *Appl. Surf. Sci.* **255**, 3868 (2009).
- ³⁵S. H. Mohamed, O. Kappertz, J. M. Ngaruiya, T. P. Leervad Pedersen, R. Drese, and M. Wuttig, *Thin Solid Films* **429**, 135 (2003).
- ³⁶A. Szekeres, T. Ivanova, and K. Gesheva, *J. Solid State Electrochem.* **7**, 17 (2002).
- ³⁷J. Tauc, R. Grigorovic, and A. Vancu, *Phys. Status Solidi* **15**, 627 (1966).
- ³⁸Z. Hussain, *J. Mater. Res.* **16**, 2695 (2001).